ISSN 1990-7931, Russian Journal of Physical Chemistry B, 2025, Vol. 19, No. 1, pp. 1–20. © Pleiades Publishing, Ltd., 2025.

STRUCTURE OF CHEMICAL COMPOUNDS, QUANTUM CHEMISTRY, SPECTROSCOPY

Molecular Structure Study of Decorated Boron Nitride Systems with Transition Metals (Cr, Ni, Zn, Mo, Pd, Cd) for Boosting Hydrogen Sorption: Nanomaterials Insight into Battery Technology

F. Mollaamin[a], * and M. Monajjemi[b]

[a] *Department of Biomedical Engineering, Faculty of Engineering and Architecture, Kastamonu University, Kastamonu, Turkey*

[b] *Department of Chemical Engineering, Central Tehran Branch, Islamic Azad University, Tehran, Iran*

**e-mail: fmollaamin@kastamonu.edu.tr*

Received April 10, 2024; revised June 27, 2024; accepted August 20, 2024

Abstract—This article wants to investigate the hydrogen storage increase through doping of the first and the second row of transition metals including Cr, Ni, Zn, Mo, Pd, Cd on the boron nitride nanocage (BNNc) has been investigated using density functional theory. The partial density of states (PDOS) can evaluate a determined charge assembly between hydrogen molecules and (Cr, Ni, Zn, Mo, Pd, Cd) → BNNc which indicates the competition among dominant complexes of transitions metals. Based on NQR analysis, nickel, and palladium with atomic charges of 0.2658 and 0.3266 coulomb on the complexes of Ni–BNNc and Pd–BNNc, respectively, have shown much more tendency for H_2 adsorption than other complexes. Furthermore, the reported results of NMR spectroscopy have exhibited that the yield of electron accepting for doping atoms on the (Cr, Ni, Zn, Mo, Pd, Cd)–BNNc through H_2 adsorption can be ordered as: Ni > Pd ⩾ Cr > Mo ≈ Zn > Cd. Regarding thermodynamic properties, it has been indicated that for a given number of hydrogen donor sites in H_2 molecules, the stabilities of complexes owing to doping atoms of Cr, Ni, Zn, Mo, Pd, Cd can be considered as: Ni–BNNc > Pd–BNNc ⩾ Cr–BNNc > Mo–BNNc ≈ Zn–BNNc > Cd–BNNc complexes. Our findings prepare important visions into the potential of employing (Cr, Ni, Zn, Mo, Pd, Cd)–BNNc nanocages in hydrogen-based energy-storage approaches. Thus, the transition metal doped BNNc can be used for designing novel materials for H_2 adsorption and sensing applications.

Keywords: hydrogen storage, BNNc, nanomaterial, doping, DFT

DOI: 10.1134/S1990793124701501

INTRODUCTION

Boron nitride nanomaterials have been used owing to their unparalleled specifications of eco-friendly attributes for pollutant adsorption and semiconducting property [1–4]. Boron nitride nanometerials usually exhibit semi-leading behavior, which is considered a proper alternative to carbon nanotubes. The properties of boron and nitrogen atoms which are the first neighbors of carbon in the periodic table, make boron nitride an interesting subject of numerous studies [5–7]. In recent years, different investigations on the adsorption of chemical contaminants and applying various boron nitride nanostructures as adsorbents for water purification have been studied [8–10].

Various physical shapes of boron nitride (BN)-based nano adsorbents such as nanoparticles, fullerenes, nanotubes, nanofibers, nanoribbons, nanosheets, nanomeshes, nanoflowers, and hollow spheres have been broadly considered possible adsorbents owing to their exceptional characteristics such as large surface area, structural variability, great chemical/mechanical strength, abundant structural defects, high reactive sites, and functional groups [11, 12]. H_2 gas is mostly preserved either by liquefaction under high compressing pressure [13–16] or by adsorption on the surface or interstitial region of material cavity [17–19]. In relation to this, the adsorption of H_2 on the surface of 2D materials has advantages in terms of safe functionality and cost-effectiveness. For the effective utilization of H_2 in fuel cells, the adsorption energy and gravimetric weight percentage on the adsorbent should be sufficiently high [20–23]. The adsorption-desorption kinetics and the strength of binding energy ought to be intermediate for hydrogen to bind on the material surfaces with an optimal adsorption energy range.

Recently, doping of transition metals containing Sc, Ti, V, Cr, Mn, Fe, Co, Ni, Cu, Zn in boron nitride nanocages has been investigated as a new method to augment the NLO response and electronic properties [24–27]. Moreover, the adsorption and sensing of H_2 and CH_2O molecules on the pristine and transition metal consisting of V, Cr, Mn, Nb, Mo, Tc, Ta, W, or Re doping on B or N site of boron nitride nanosheets. The achieved results exhibit that the pristine BNNS

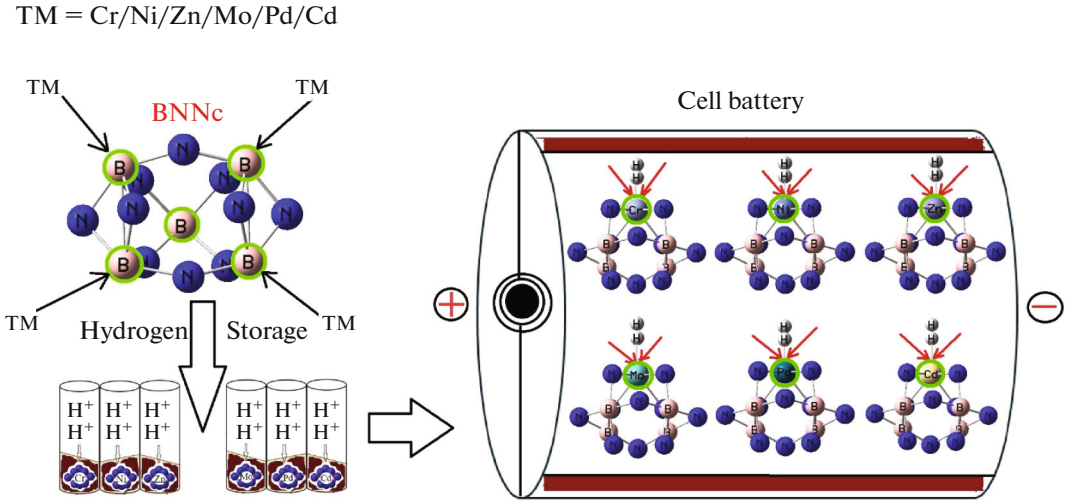

Fig. 1. Application of (Cr, Ni, Zn, Mo, Pd, Cd)–BNNc for adsorption of hydrogen molecules in the energy storage accompanying formation of complexes: $H_2 \rightarrow$ Cr–BNNc, $H_2 \rightarrow$ Ni–BNNc, $H_2 \rightarrow$ Zn–BNNc, $H_2 \rightarrow$ Mo–BNNc, $H_2 \rightarrow$ Pd–BNNc, and $H_2 \rightarrow$ Cd–BNNc complexes using CAM–B3LYP–D3/6-311+G(*d*, *p*), LANL2DZ calculation.

indicates fragile interaction with the H_2 and CH_2O molecules. The H_2 and CH_2O molecules might be strongly adsorption on the transition metal doped BNNSs with appreciable adsorption energy through the geometrical deformation on the transition metal doping zone [28–31]. Boron nitride doped with the transition metal presents strong material candidature for flexible magnetic memory chips that are functional even under fire. Besides, spin-polarized density functional theory band structure calculations can approve clear spin asymmetry due to doping [32–39].

Owing to the obvious reasons mentioned above, we have explored the possibility of using boron nitride nanocages doped with chromium, nickel, zinc, molybdenum, palladium, and cadmium for H_2 storage by employing first-principles calculations. We have analyzed the structural and electronic properties of (Cr, Ni, Zn, Mo, Pd, Cd)–BNNc nanocages using state-of-the-art computational techniques. Particularly, this research work aims to assess the influences of doping atoms of Cr, Ni, Zn, Mo, Pd, Cd on the BNNc for increasing hydrogen detection through measurement of some parameters containing charge transfer, electric potential, electromagnetic and thermodynamic properties, surface area, functional group and examine the ability of applying (Cr, Ni, Zn, Mo, Pd, Cd)–BNNc nanocages in hydrogen-based energy-storage approaches.

THEORY, MATERIALS AND METHOD

The aim of this study is to adsorb hydrogen molecules by using (Cr, Ni, Zn, Mo, Pd, Cd)-doped BNNc (Fig. 1). Boron nitride nanocage was modeled in the presence of doping atoms of chromium, nickel, zinc, molybdenum, palladium, and cadmium which can increase the hydrogen sensing potential of BN-nanocage. In our research, the calculations have been done by CAM–B3LYP–D3 /EPR–3, LANL2DZ level of theory.

Figure 1 has shown the process adsorption of H_2 molecules on the (Cr, Ni, Zn, Mo, Pd, Cd)–BNNc surface which towards formation of complexes containing

$$\text{H–H} \rightarrow \text{Cr–BNNc}, \quad \text{H–H} \rightarrow \text{Ni–BNNc},$$
$$\text{H–H} \rightarrow \text{Zn–BNNc}, \quad \text{H–H} \rightarrow \text{Mo–BNNc},$$
$$\text{H–H} \rightarrow \text{Pd–BNNc}, \text{ and } \text{H–H} \rightarrow \text{Cd–BNNc},$$

complexes by molecular modeling computations. The charge distribution of mentioned complexes is calculated due to the Bader charge analysis [40]. The trapping of H_2 molecules by (Cr, Ni, Zn, Mo, Pd, Cd)–BNNc were successfully incorporated due to binding formation consisting of

$$\text{H–H} \rightarrow \text{Cr–BNNc}, \quad \text{H–H} \rightarrow \text{Ni–BNNc},$$
$$\text{H–H} \rightarrow \text{Zn–BNNc}, \quad \text{H–H} \rightarrow \text{Mo–BNNc},$$
$$\text{H–H} \rightarrow \text{Pd–BNNc},$$

and

$$\text{H–H} \rightarrow \text{Cd–BNNc},$$

complexes (Fig. 1).

In this article, the rigid potential energy surface (PES) using DFT [41–54] calculations have been computed applying Gaussian 16 revision C.01 software [55]. The input Z-matrix for adsorption of H_2 molecules by the (Cr, Ni, Zn, Mo, Pd, Cd)–BNNc has been designed with GaussView 6.1 [56] using 6-311+G(*d*, *p*), EPR–3, LANL2DZ basis set. In this study, the interaction between H_2 molecules and (Cr, Ni, Zn, Mo, Pd, Cd)–BNNc was modeled and analyzed. As revealed by DFT-based analysis, the potency

of (Cr, Ni, Zn, Mo, Pd, Cd)–BNNc for grabbing H_2 molecules was determined mainly by the electronegativity of the functional groups, as well as the interaction between the (Cr, Ni, Zn, Mo, Pd, Cd)–BNNc and the H_2 molecules. In our previous works, it has been accomplished application of DFT calculations through materials modelling [57–60].

RESULTS AND DISCUSSION

In this article, the data has evaluated the efficiency of boron nitride nanocage doped with chromium, nickel, zinc, molybdenum, palladium, and cadmium for hydrogen detection. In fact, it can be remarked the chemisorptive nature of the bond among the hydrogen molecules with boron and nitrogen elements through the equilibrium distribution of doping atoms, BNNc, and a monolayer attribute.

PDOS and Electronic Evaluating

The electronic structures of hydrogen adsorption on the (Cr, Ni, Zn,Mo, Pd, Cd)-doped BNNc have been illustrated using CAM–B3LYP–D3/6-311+G(*d*, *p*), LANL2DZ level of theory. Figure 2 shows the projected density of state (PDOS) of $H_2 \rightarrow$ (Cr, Ni, Zn, Mo, Pd, Cd)–BNNc through hydrogen molecules adsorption. The appearance of the energy states (*d*-orbital) of Cr, Ni, Zn, Mo, Pd, Cd within the gap of (Cr, Ni, Zn, Mo, Pd, Cd)–BNNc induces the reactivity of the system. It is clear from the figure that after trapping with hydrogen molecules, there is a significant contribution of *p*-orbitals of N and B in the unoccupied level of BNNc. Therefore, the curve of partial PDOS has described the *s* states of H atoms and *d*-orbitals of Cr, Ni, Zn, Mo, Pd, Cd atoms in (Cr, Ni, Zn, Mo, Pd, Cd)–BNNc overcome due to the conduction band. A distinguished adsorption trait might be seen in $H_2 \rightarrow$ (Cr, Ni, Zn, Mo, Pd, Cd)–BNNc because of the potent interaction between the *s* states of hydrogen atoms with *d* states of Cr, Ni, Zn, Mo, Pd, Cd in TM–BNNc complexes. It has been shown that

$$H_2 \rightarrow \text{Cr–BNNc}, \quad H_2 \rightarrow \text{Ni–BNNc},$$
$$H_2 \rightarrow \text{Zn–BNNc}, \quad H_2 \rightarrow \text{Mo–BNNc},$$
$$H_2 \rightarrow \text{Pd–BNNc},$$

and

$$H_2 \rightarrow \text{Cd–BNNc},$$

complexes through hydrogen adsorption, respectively, have the most contribution at the middle of the conduction band between −5 to −10 eV, while contribution of boron and nitrogen states are enlarged and similar together, and adsorbing of H_2 depicts interfacial electronic of the BNNc for selection of hydrogen molecules. $H_2 \rightarrow$ Cr–BNNc has indicated sharp peaks for Cr atom close to H atoms in Fig. 2a. $H_2 \rightarrow$ Ni– BNNc (Fig. 2b) has exhibited strong peaks for Ni atom close to H atoms. Furthermore, the sharp Zn graph near H atoms in $H_2 \rightarrow$ Zn–BNNc (Fig. 2c) has been indicated. $H_2 \rightarrow$ Mo–BNNc has indicated sharp peaks for Cr atom close to H atoms in Fig. 2d. $H_2 \rightarrow$ Pd–BNNc (Fig. 2e) has exhibited strong peaks for Ni atom close to H atoms. Furthermore, the sharp Zn graph near H atoms in $H_2 \rightarrow$ Cd–BNNc (Fig. 2f) has been indicated. Therefore, the order ability of hydrogen adsorption by doping atoms of Cr, Ni, Zn, Mo, Pd, Cd on BNNc based on the PDOS might be shifted as:

$$\text{Ni–BNNc} > \text{Pd–BNNc} > \text{Cr–BNNc}$$
$$> \text{Mo–BNNc} \approx \text{Zn–BNNc} > \text{Cd–BNNc}.$$

Insight to Nuclear Quadrupole Resonance

As the electric field gradient (EFG) at the citation of the nucleus in H_2 is allocated by the valence electrons twisted in the attachment with close nuclei of (Cr, Ni, Zn, Mo, Pd, Cd)–BNNc through trapping of hydrogen molecules, the nuclear quadrupole resonance (NQR) frequency at which transitions occur is particular for $H_2 \rightarrow$ (Cr, Ni, Zn, Mo, Pd, Cd)–BNNc complexes (Table 1) [61–64]. In this research work, the electric potential as the quantity of work energy through carrying over the electric charge from one position to another position in the essence of electric field has been evaluated for

$$H_2 \rightarrow \text{Cr–BNNc}, \quad H_2 \rightarrow \text{Ni–BNNc},$$
$$H_2 \rightarrow \text{Zn–BNNc}, \quad H_2 \rightarrow \text{Mo–BNNc},$$
$$H_2 \rightarrow \text{Pd–BNNc},$$

and

$$H_2 \rightarrow \text{Cd–BNNc},$$

complexes (Table 1).

In Table 1, the Bader charge and electronic potential properties of (Cr, Ni, Zn, Mo, Pd, Cd)–B, N and hydrogen molecules absorbed on atom–doped boron nitride nanocage have been investigated. The amounts indicate that with increasing the negative charge of different atoms, the electric potential resulted from NQR calculations increase. Moreover, the doping atoms of Cr13, Ni13, Zn13, Mo13, Pd13, Cd13 on the BNNc have shown the most potential for accepting the electron from electron donor of H (16) and H (17) in H_2 adsorbed on the BNNc (Table 1). Furthermore, in Fig. 3, it has been sketched the electric potential of nuclear quadrupole resonance for some atoms of (Cr, Ni, Zn, Mo, Pd, Cd)/B, N and H atoms of H_2 molecule trapped on atom-doped boron nitride nanocage which has been calculated by CAM–B3LYP–D3/EPR-3, LANL2DZ.

In Fig. 3a, it was observed the behavior of H_2 adsorption on the Cr–BNNc with high sensitivity based on relation coefficient of $R^2 = 0.9875$. Adsorption of H_2 on the Ni–BNNc and in Fig. 3b has illustrated

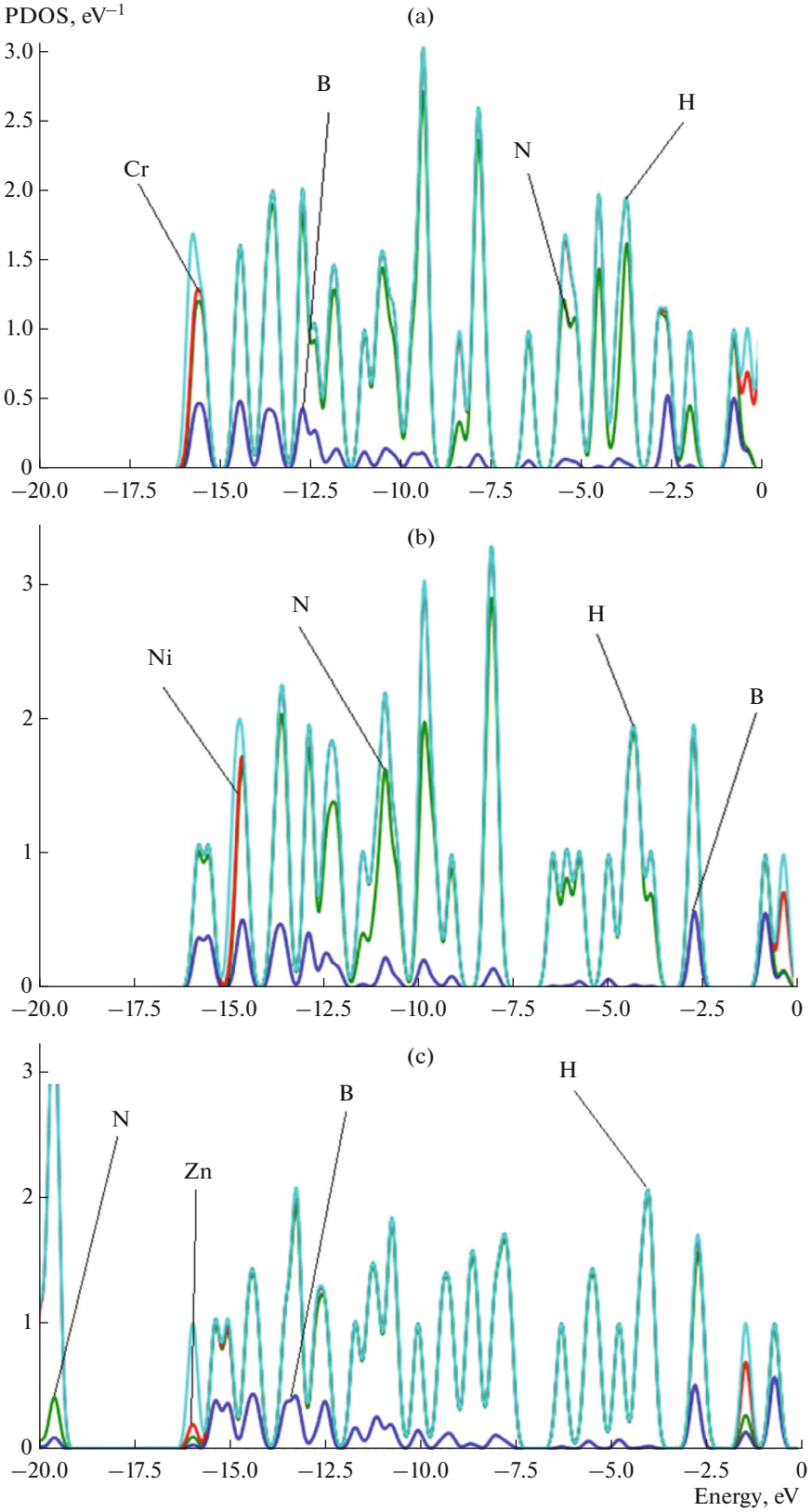

Fig. 2. PDOS of H_2 adsorbed on (Cr, Ni, Zn, Mo, Pd, Cd)–BNNc toward formation of (a) H_2 → Cr–BNNc, (b) H_2 → Ni–BNNc, (c) H_2 → Zn–BNNc, (d) H_2 → Mo–BNNc, (e) H_2 → Pd–BNNc, and (f) H_2 → Cd–BNNc complexes by CAM–B3LYP–D3/6–311+G(*d*, *p*), LANL2DZ.

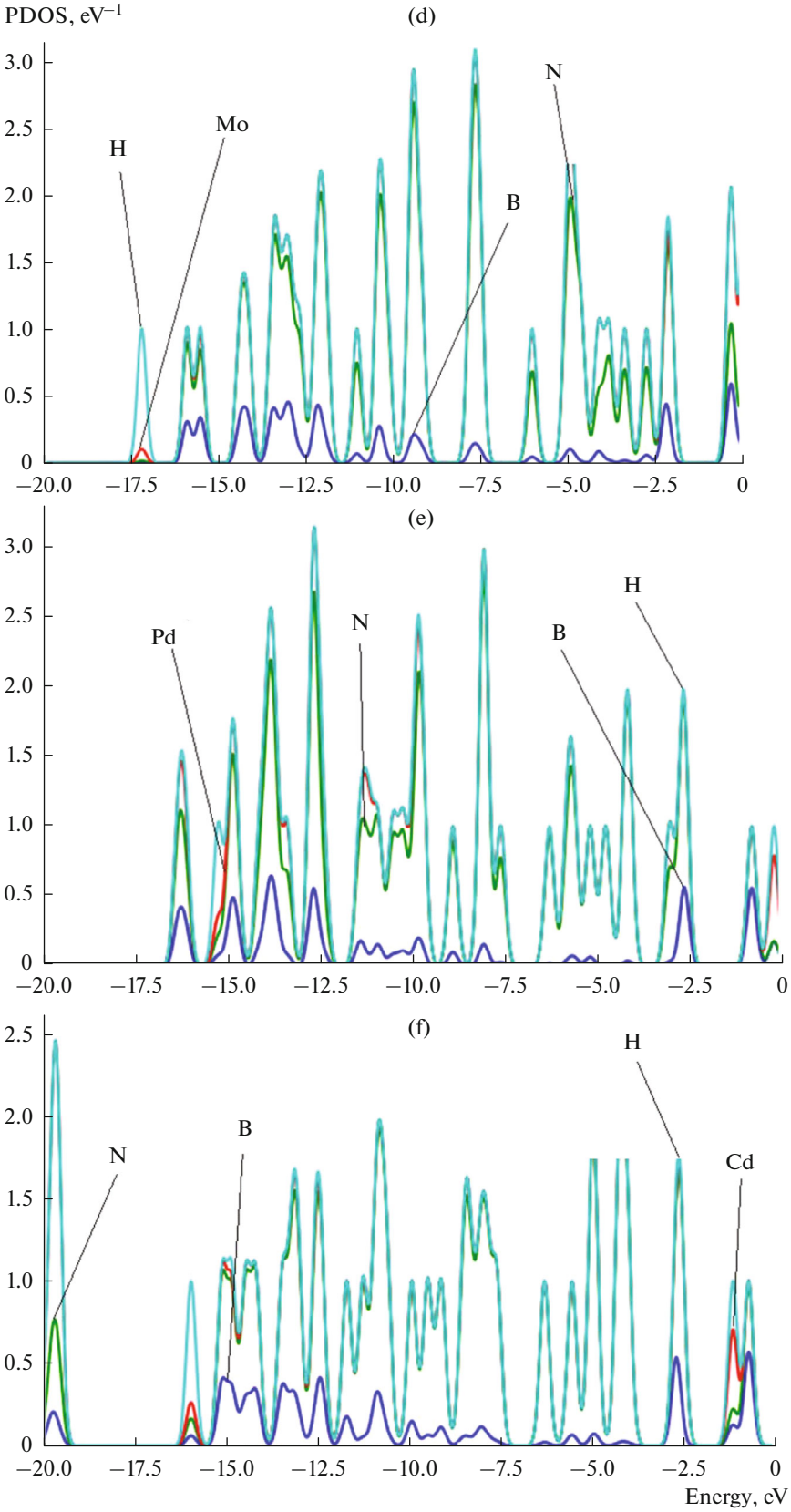

Fig. 2. (Contd.)

Table 1. The electric potential (E_p/a.u.) and Bader charge (Q/coulomb) through NQR calculation for $H_2 \rightarrow$ Cr–BNNc, $H_2 \rightarrow$ Ni–BNNc, $H_2 \rightarrow$ Zn–BNNc, $H_2 \rightarrow$ Mo–BNNc, $H_2 \rightarrow$ Pd–BNNc, and $H_2 \rightarrow$ Cd–BNNc complexes using CAM–B3LYP–D3/6-311+G(*d*, *p*), LANL2DZ calculation

H–H → Cr–BNNc			H–H → Ni–BNNc			H–H → Zn–BNNc		
atom	*Q*	E_p	atom	*Q*	E_p	atom	*Q*	E_p
B1	0.13	−11.28	B1	0.15	−11.29	B1	0.11	−11.29
N2	−0.06	−18.29	N2	−0.06	−18.28	N2	−0.04	−18.29
N3	−0.11	−18.30	N3	−0.06	−18.26	N3	−0.07	−18.26
B4	0.13	−11.28	B4	0.15	−11.29	B4	0.11	−11.29
B5	0.13	−11.29	B5	0.14	−11.29	B5	0.11	−11.29
B6	0.13	−11.29	B6	0.14	−11.29	B6	0.11	−11.29
N7	−0.04	−18.27	N7	−0.08	−18.29	N7	−0.06	−18.28
N8	−0.11	−18.30	N8	−0.06	−18.26	N8	−0.07	−18.26
N9	−0.19	−18.28	N9	−0.13	−18.27	N9	−0.26	−18.29
N10	−0.19	−18.28	N10	−0.13	−18.27	N10	−0.26	−18.29
N11	−0.19	−18.28	N11	−0.13	−18.27	N11	−0.26	−18.29
N12	−0.19	−18.28	N12	−0.13	−18.27	N12	−0.26	−18.29
Cr13	0.61	−14.44	Ni13	0.26	−23.55	Zn13	0.86	−16.16
N14	−0.04	−18.27	N14	−0.08	−18.30	N14	−0.06	−18.28
N15	−0.06	−18.29	N15	−0.06	−18.28	N15	−0.04	−18.29
H16	−0.15	−1.00	H16	−0.07	−1.03	H16	−0.13	−0.99
H17	0.22	−0.97	H17	0.16	−1.01	H17	0.22	−0.95
H–H →Mo–BNNc			H–H → Pd–BNNc			H–H → Cd–BNNc		
atom	*Q*	E_p	atom	Q	E_p	atom	Q	E_p
B1	0.13	−11.30	B1	0.14	−11.29	B1	0.12	−11.30
N2	−0.09	−18.31	N2	−0.07	−18.29	N2	−0.05	−18.30
N3	−0.05	−18.30	N3	−0.07	−18.27	N3	−0.07	−18.26
B4	0.13	−11.30	B4	0.14	−11.29	B4	0.12	−11.30
B5	0.13	−11.30	B5	0.14	−11.29	B5	0.12	−11.30
B6	0.13	−11.30	B6	0.14	−11.29	B6	0.11	−11.30
N7	−0.10	−18.32	N7	−0.07	−18.29	N7	−0.06	−18.29
N8	−0.05	−18.30	N8	−0.07	−18.27	N8	−0.07	−18.26
N9	−0.27	−18.30	N9	−0.13	−18.27	N9	−0.19	−18.30
N10	−0.28	−18.30	N10	−0.13	−18.27	N10	−0.19	−18.30
N11	−0.28	−18.29	N11	−0.13	−18.27	N11	−0.19	−18.30
N12	−0.27	−18.29	N12	−0.13	−18.27	N12	−0.19	−18.30
Mo13	1.04	−10.59	Pd13	0.32	−16.16	Cd13	0.61	−10.04
N14	−0.10	−18.32	N14	−0.08	−18.29	N14	−0.06	−18.29
N15	−0.09	−18.31	N15	−0.07	−18.29	N15	−0.05	−18.30
H16	−0.27	−0.95	H16	−0.07	−1.02	H16	−0.10	−0.99
H17	0.30	−0.91	H17	0.16	−1.01	H17	0.19	−0.96

the highest sensing of $R^2 = 1$. In addition, Fig. 3c has resulted that Zn–BNNc has a good detecting for H_2 adsorption based on the relation coefficient of $R^2 = 0.975$. In Fig. 3d, it was observed the behavior of H_2 adsorption on the Mo–BNNc with high sensitivity based on relation coefficient of $R^2 = 0.9781$. Adsorption of H_2 on the Pd–BNNc and in Fig. 3e has illustrated the highest sensing of $R^2 = 0.9709$. In addition, Fig. 3f has

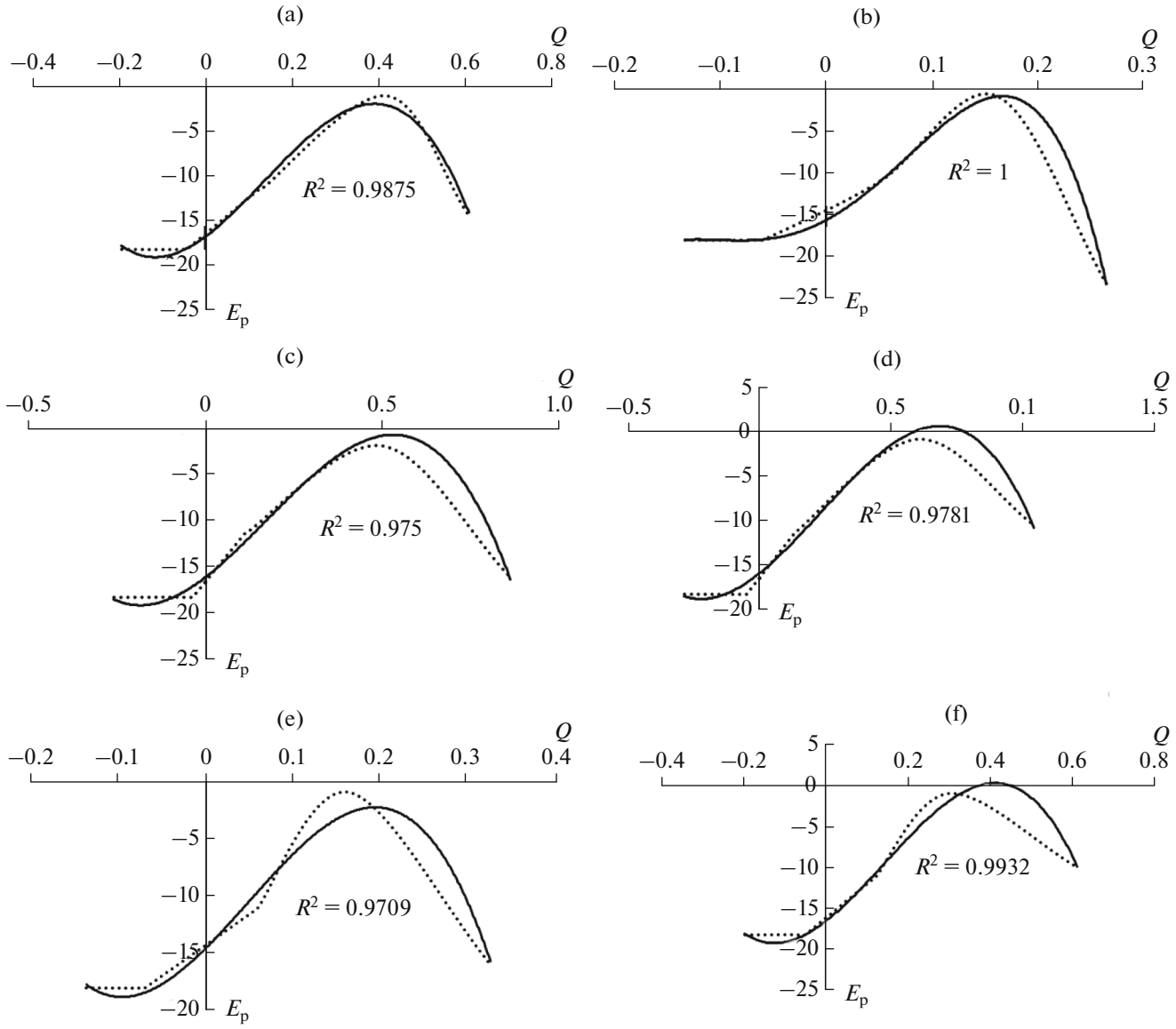

Fig. 3. Electric potential (a.u.) versus Bader charge (coulomb) through NQR calculation for (a) $H_2 \rightarrow$ Cr–BNNc, (b) $H_2 \rightarrow$ Ni–BNNc, (c) $H_2 \rightarrow$ Zn–BNNc, (d) $H_2 \rightarrow$ Mo–BNNc, (e) $H_2 \rightarrow$ Pd–BNNc, and (f) $H_2 \rightarrow$ Cd–BNNc complexes by CAM–B3LYP–D3/EPR-3, LANL2DZ.

resulted that Cd– BNNc has a good detecting for H_2 adsorption based on the relation coefficient of $R^2 = 0.9932$.

It's vivid that the curve of (Cr, Ni, Zn, Mo, Pd, Cd)–BNNc is waved by these H_2 molecules. The fluctuated peaks for electric potential have been shown around H_2 trapping on the (Cr, Ni, Zn, Mo, Pd, Cd)–BNNc which demonstrates the electron accepting specifications of hydrogen versus the chromium, nickel, zinc, molybdenum, palladium, and cadmium doped on the BNNc. Besides, it can be considered that nickel (Fig. 3b) and cadmium (Fig. 3f) as the first and second row of transitions metals in the periodic table, respectively, in the functionalized BNNc might have more impressive sensitivity for accepting the electrons from H atoms in the process of adsorption mechanism. However, molybdenum-doped on BNNc (adsorbent) has shown the lowest fluctuation ($R^2 = 0.9781$) between Bader charge versus electric potential extracted from NQR parameters and the lowest negative atomic charge including 1.0432 coulomb on the Mo– BNNc complex which has the lowest tendency for H_2 adsorption after Zn with 0.8620 coulomb on the Zn–BNNc complex and Cr or Cd with 0.6093 coulomb on the Cr–BNNc or Cd–BNNc complexes (Table 1). Nickel and palladium with atomic charges of 0.2658 and 0.3266 coulomb on the complexes of Ni–BNNc and Pd–BNNc, respec-

tively, have shown much more tendency for H_2 adsorption than other complexes. In fact, the uptake of H_2 molecules has been known to be associated with (Cr, Ni, Zn, Mo, Pd, Cd)–BNNc, indicating that the adsorbed hydrogen molecules in the (Cr, Ni, Zn, Mo, Pd, Cd)-doped nanocage can be internalized through a different pathway from pristine nanocage.

Analysis of Nuclear Magnetic Resonance Spectra

Based on the resulted amounts, nuclear magnetic resonance (NMR) spectrums of (Cr, Ni, Zn, Mo, Pd, Cd)–BNNc complexes as the potential molecules for H_2 storage can unravel the efficiency of (Cr, Ni, Zn, Mo, Pd, Cd)–BNNc for saving clean energy. From the DFT calculations, it has been attained the chemical shielding (CS) tensors in the principal axes system to estimate the isotropic chemical-shielding (CSI) and anisotropic chemical-shielding (CSA) [65–71]. The NMR data of isotropic (σ_{iso}) and anisotropic shielding tensors (σ_{aniso}) of hydrogen molecules trapped in the (Cr, Ni, Zn, Mo, Pd, Cd)–BNNc towards formation of

$$H_2 \rightarrow Cr\text{–}BNNc,\quad H_2 \rightarrow Ni\text{–}BNNc,$$
$$H_2 \rightarrow Zn\text{–}BNNc,\quad H_2 \rightarrow Mo\text{–}BNNc,$$
$$H_2 \rightarrow Pd\text{–}BNNc,$$

and

$$H_2 \rightarrow Cd\text{–}BNNc,$$

complexes have been computed by Gaussian 16 revision C.01 program package [55] and been shown in Table 2.

In Table 2, NMR data has reported the notable amounts for H_2 molecules which were adsorbed on the (Cr, Ni, Zn, Mo, Pd, Cd)–BNNc. The observed increase in the chemical shift anisotropy spans for H atoms adsorption on the (Cr, Ni, Zn, Mo, Pd, Cd)–BNNc are near N2, N3, N7, N8, N14 and N15. The observed weak signal intensity near the parallel edge of the nanocage pattern may be due to boron binding induced non-spherical distribution of these complexes. It is remarkable that doping of Cr, Ni, Zn, Mo, Pd, Cd on BNNc might promote the stability of nanocage that results in enhanced magnetic alignment of complexes. Interestingly, the reported results show that Cr, Ni, Zn, Mo, Pd, Cd elements can be optimized to achieve optimal alignment of nanocage in the presence of an applied magnetic field. Figure 4 exhibited the same tendency of shielding for boron and nitrogen; however, a considerable deviation exists from doping atoms of Cr13, Ni13, Zn13, Mo13, Pd13, Cd13 through interaction with H16 and H17 of H_2 molecules during adsorbing on the BNNc pristine. H_2 molecules in the complexes of $H_2 \rightarrow$ Cr–BNNc (Fig. 4a), $H_2 \rightarrow$ Ni–BNNc (Fig. 4b), $H_2 \rightarrow$ Zn–BNNc (Fig. 4c), $H_2 \rightarrow$ Mo–BNNc (Fig. 4d), $H_2 \rightarrow$ Pd–BNNc (Fig. 4e), and $H_2 \rightarrow$ Cd–BNNc (Fig. 4f) denote the fluctuation in the chemical shielding during ion trapping. Figure 4 shows the gap chemical shielding between chromium, nickel, zinc, molybdenum, palladium, and cadmium doping of (Cr, Ni, Zn, Mo, Pd, Cd)–BNNc complexes and hydrogen molecules. The yield of electron accepting for doping atoms on the (Cr, Ni, Zn, Mo, Pd, Cd)–BNNc complexes through hydrogen molecules adsorption can be ordered as:

$$Ni > Pd \gg Cr > Mo \approx Zn > Cd,$$

that approves the possibility of covalent bond between chromium, nickel, zinc, molybdenum, palladium, and cadmium, and hydrogen atoms in H_2 molecules towards energy storage in battery technology.

In the NMR spectroscopy, it has been observed the remarkable peaks around interaction of H_2 molecules through adsorbing on the (Cr, Ni, Zn, Mo, Pd, Cd)–BNNc during molecule detection; however, there are some fluctuations in the chemical shielding behaviors of isotropic and anisotropy attributes. Therefore, the authors believe that the extracted results would be useful in the design of (Cr, Ni, Zn, Mo, Pd, Cd)–BNNc based doped nanomaterials for increasing the adsorption of hydrogen molecules in addition to the structural studies using solid-state and solution NMR technique.

Infrared Spectroscopy and Thermodynamic Factors

The infrared (IR) calculations have been accomplished for adsorption of H_2 molecules by (Cr, Ni, Zn, Mo, Pd, Cd)–BNNc during hydrogen sensing. Therefore, it has been simulated the several clusters containing $H_2 \rightarrow$ Cr–BNNc (Fig. 5a), $H_2 \rightarrow$ Ni–BNNc (Fig. 5b), $H_2 \rightarrow$ Zn–BNNc (Fig. 5c), $H_2 \rightarrow$ Mo–BNNc (Fig. 5d), $H_2 \rightarrow$ Pd–BNNc (Fig. 5e), and $H_2 \rightarrow$ Cd–BNNc (Fig. 5f) using CAM–B3LYP–D3/6-311+G(*d*, *p*), LANL2DZ.

The graph of Fig. 5a has been observed in the frequency range between 100–1100 cm^{-1} for $H_2 \rightarrow$ Cr–BNNc with several sharp peaks around 370.79, 506.23, 582.86, 606.67, 750.79 and 827.10 cm^{-1}. Figure 5b has shown the frequency range between 50–1200 cm^{-1} for $H_2 \rightarrow$ Ni–BNNc with sharp peaks around 77.24, 114.98, 244.25, 573.88, and 718.47 cm^{-1}. Figure 5c has indicated the fluctuation of frequency between 500–5100 cm^{-1} for $H_2 \rightarrow$ Zn–BNNc with sharp peaks around 173.84, 567.81, 663.90, and 5089.68 cm^{-1}. The graph of Fig. 5d has been observed in the frequency range between 100–1200 cm^{-1} for $H_2 \rightarrow$ Mo–BNNc with several sharp peaks around 393.04, 604.51, 736.86, 832.58 and 1109.51 cm^{-1}. Figure 5e shows the frequency range between 100–1200 cm^{-1} for $H_2 \rightarrow$ Pd–BNNc with sharp peaks around 148.81, 327.29, 563.40, and 734.87 cm^{-1}. Figure 5f has indicated

Table 2. Data of NMR shielding tensors (ppm) for selected atoms of $H_2 \rightarrow$ Cr–BNNc, $H_2 \rightarrow$ Ni–BNNc, $H_2 \rightarrow$ Zn–BNNc, $H_2 \rightarrow$ Mo–BNNc, $H_2 \rightarrow$ Pd–BNNc, and $H_2 \rightarrow$ Cd–BNNc complexes using CAM–B3LYP–D3/6-311+G(*d*, *p*), LANL2DZ calculation

H–H → Cr–BNNc			H–H → Ni–BNNc			H–H → Zn–BNNc		
atom	σ_{iso}	σ_{aniso}	atom	σ_{iso}	σ_{aniso}	atom	σ_{iso}	σ_{aniso}
B1	70.26	58.79	B1	300.63	683.37	B1	68.94	212.51
N2	1365.30	2043.33	N2	7410.91	44923.50	N2	7461.99	8805.66
N3	619.51	1587.38	N3	8440.90	22135.34	N3	5626.33	19678.42
B4	70.11	60.27	B4	300.31	682.33	B4	68.59	214.13
B5	68.86	57.35	B5	300.37	684.01	B5	67.06	212.56
B6	68.53	59.86	B6	300.21	683.57	B6	67.39	213.38
N7	68.18	584.89	N7	3333.70	21040.92	N7	3095.82	14805.57
N8	118.72	1254.15	N8	8510.96	22312.55	N8	5726.78	19580.01
N9	435.37	1453.12	N9	1569.82	9173.70	N9	598.19	8738.028
N10	459.72	1446.93	N10	1588.75	9023.92	N10	594.40	8734.551
N11	440.91	1402.27	N11	1595.17	9119.80	N11	573.76	8745.053
N12	458.75	1487.02	N12	1560.47	9091.05	N12	572.00	8647.37
Cr13	15044.24	7802.68	Ni13	29284.05	56000.40	Zn13	248.78	2109.01
N14	61.85	594.18	N14	3335.62	21081.45	N14	3103.05	14779.11
N15	1348.21	2093.25	N15	7432.71	44860.24	N15	7514.91	8838.80
H16	61.27	101.12	H16	53.13	151.90	H16	45.21	75.75
H17	34.49	32.28	H17	0.56	48.77	H17	31.97	36.68
H–H → Mo– BNNc			H–H → Pd– BNNc			H–H → Cd– BNNc		
Atom	σ_{iso}	σ_{aniso}	atom	σ_{iso}	σ_{aniso}	atom	σ_{iso}	σ_{aniso}
B1	59.53	58.91	B1	96.36	168.36	B1	66.753	105.22
N2	534.84	2068.89	N2	3381.37	7908.529	N2	3343.74	3860.29
N3	419.12	4987.96	N3	1029.00	1121.605	N3	2534.35	6807.29
B4	62.28	60.60	B4	96.34	167.9665	B4	66.65	105.44
B5	61.85	84.96	B5	95.32	166.3486	B5	66.34	105.65
B6	61.32	91.14	B6	95.31	166.2311	B6	66.36	105.62
N7	375.18	1463.34	N7	571.00	3385.67	N7	585.26	5978.95
N8	3129.08	9298.23	N8	1062.70	1136.304	N8	2550.21	6802.59
N9	656.82	876.56	N9	37.25	3835.706	N9	35.21	3556.65
N10	639.76	778.04	N10	44.35	4015.94	N10	39.29	3557.94
N11	661.95	775.09	N11	42.93	4027.371	N11	34.05	3566.06
N12	643.49	844.80	N12	35.01	3825.071	N12	31.18	3532.10
Mo13	1131.98	514.15	Pd13	1115.05	1036.646	Cd13	243.95	307.64
N14	418.69	1345.76	N14	571.55	3384.7	N14	586.65	5973.05
N15	527.86	1989.27	N15	3382.21	7909.511	N15	3351.76	3863.72
H16	1989.27	62.68	H16	23.53	45.3175	H16	42.98	23.69
H17	26.89	21.99	H17	21.39	7.3431	H17	31.48	13.10

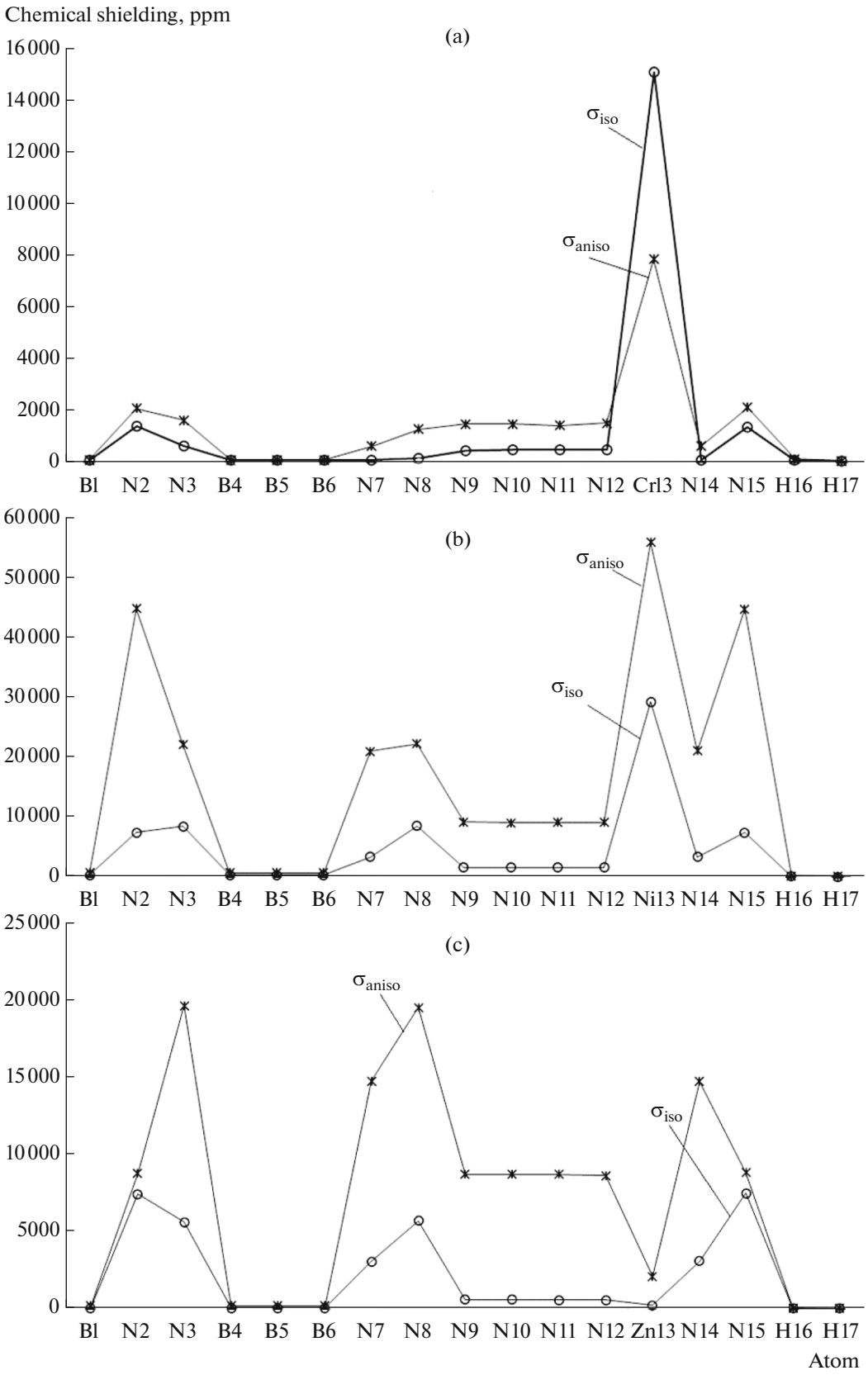

Fig. 4. The NMR spectra for (a) $H_2 \rightarrow$ Cr–BNNc, (b) $H_2 \rightarrow$ Ni–BNNc, (c) $H_2 \rightarrow$ Zn–BNNc, (d) $H_2 \rightarrow$ Mo–BNNc, (e) $H_2 \rightarrow$ Pd–BNNc, and (f) $H_2 \rightarrow$ Cd–BNNc complexes using CAM–B3LYP–D3/6–311+G(*d*, *p*), LANL2DZ.

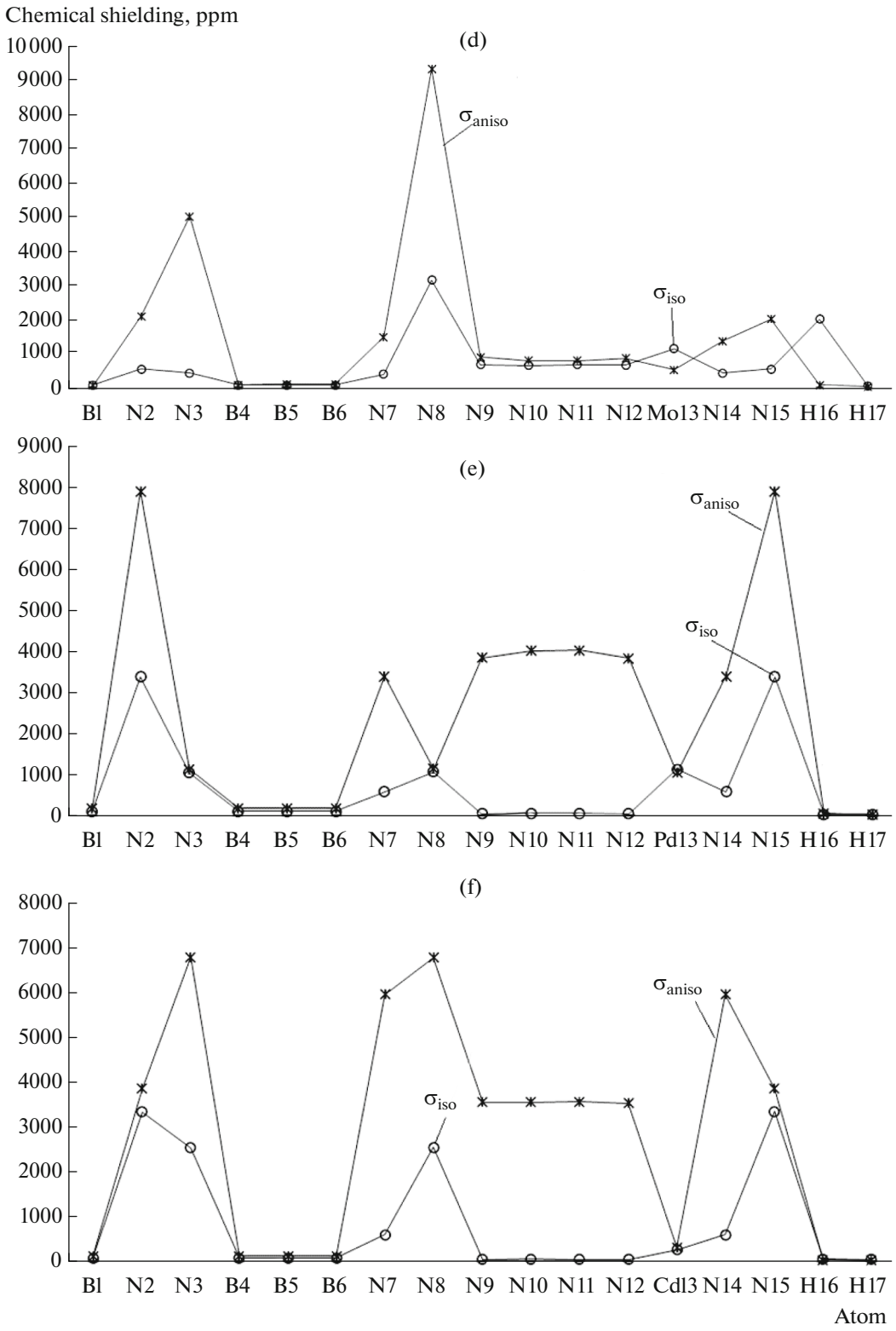

Fig. 4. (Contd.)

the fluctuation of frequency between 100–5200 cm^{-1} for $H_2 \rightarrow$ Cd–BNNc with sharp peaks around 303.53, 548.81, 569.92, 674.82 and 5122.66 cm^{-1}.

The IR spectra of H_2 adsorption with (Cr, Ni, Zn, Mo, Pd, Cd)–BNNc has demonstrated that the structure of the dominant complex correlates with the elec-

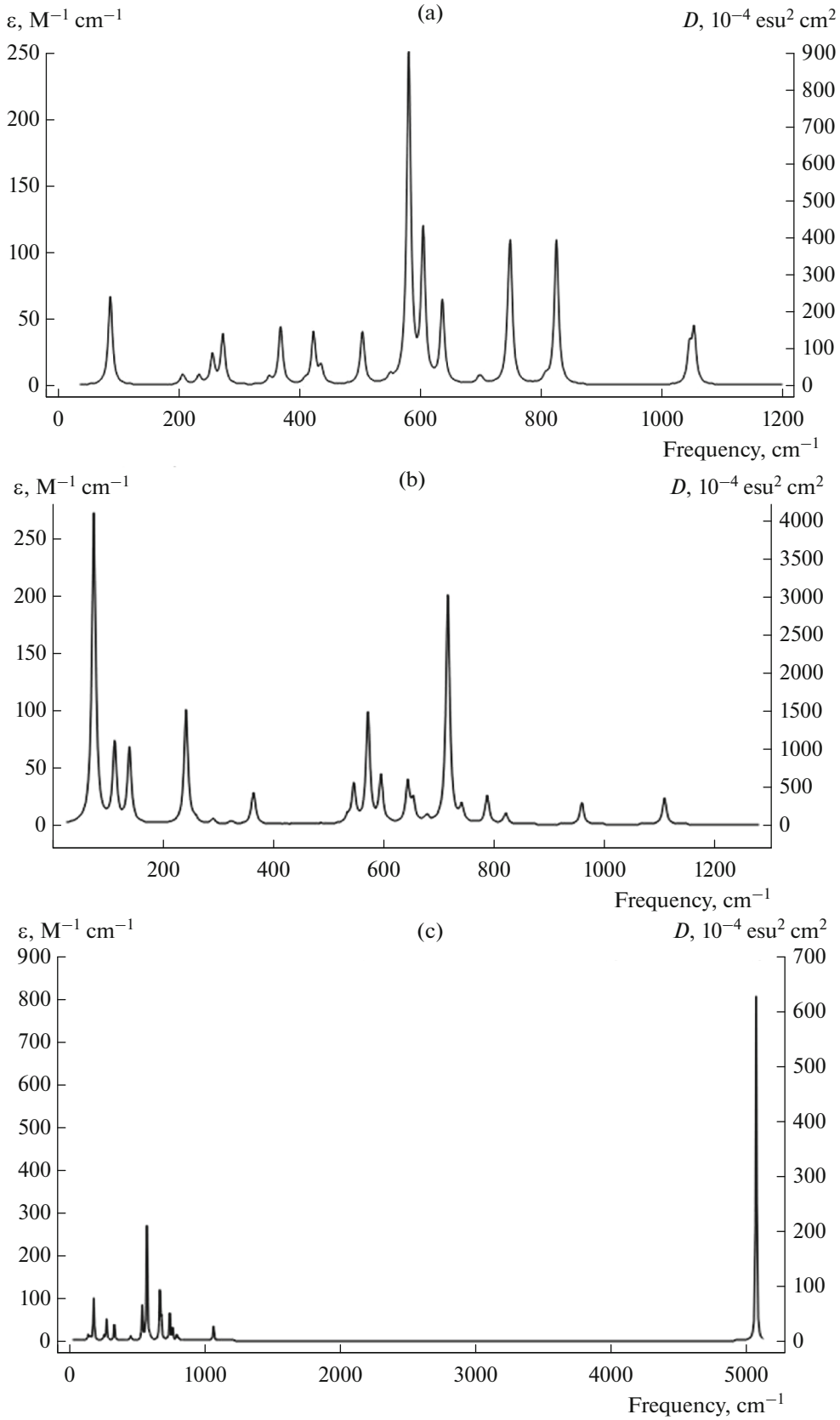

Fig. 5. The frequency (cm^{-1}) changes through the IR spectra for (a) $H_2 \rightarrow$ Cr–BNNc, (b) $H_2 \rightarrow$ Ni–BNNc, (c) $H_2 \rightarrow$ Zn–BNNc, (d) $H_2 \rightarrow$ Mo–BNNc, (e) $H_2 \rightarrow$ Pd–BNNc, and (f) $H_2 \rightarrow$ Cd–BNNc complexes using CAM–B3LYP–D3/6-311+G(*d*, *p*), LANL2DZ.

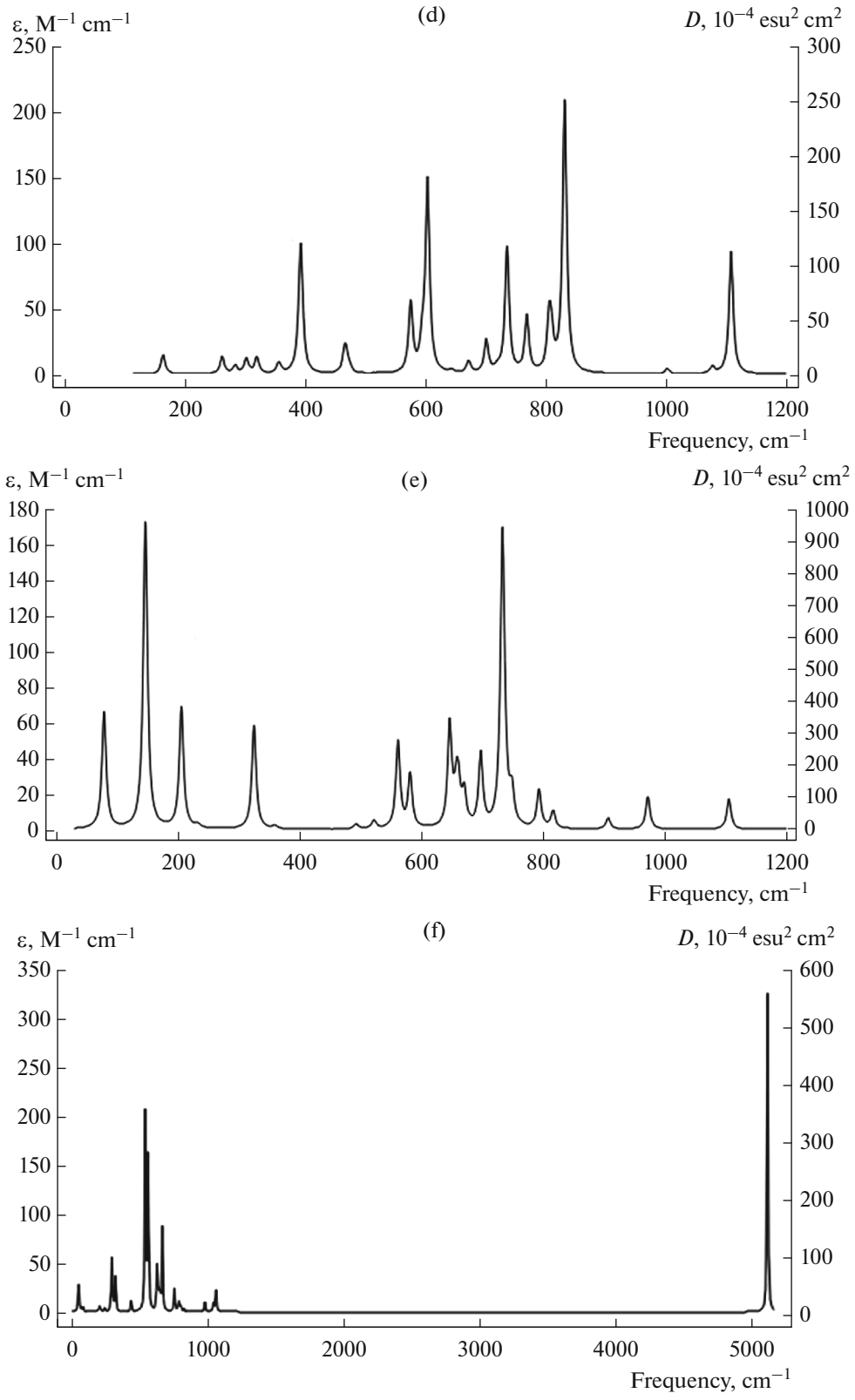
(d)
ε, M^{-1} cm^{-1}
D, 10^{-4} esu^2 cm^2
Frequency, cm^{-1}
(e)
ε, M^{-1} cm^{-1}
D, 10^{-4} esu^2 cm^2
Frequency, cm^{-1}
(f)
ε, M^{-1} cm^{-1}
D, 10^{-4} esu^2 cm^2
Frequency, cm^{-1}

Fig. 5. (Contd.)

Table 3. The thermodynamic characters of H_2 adsorption on the Cr–BNNc, Ni–BNNc, $H_2 \rightarrow$ Zn–BNNc, Mo–BNNc, Pd–BNNc, and Cd–BNNc complexes using CAM–B3LYP–D3/6-311+G(*d*, *p*), LANL2DZ calculation.

Compound	Dipole moment, Debye	$\Delta E^{o}_{ads} \times 10^{-3}$, kcal/mol	$\Delta H^{o}_{ads} \times 10^{-3}$, kcal/mol	$\Delta G^{o}_{ads} \times 10^{-3}$, kcal/mol	ΔS^{o}_{ads}, cal/K mol
BNNc pristine	0.20	–420.55	–420.55	–420.58	100.65
Cr–BNNc	3.68	–459.20	–459.20	–459.23	98.70
Ni–BNNc	1.90	–511.24	–494.94	–511.27	99.66
Zn–BNNc	3.40	–446.11	–446.11	–446.14	104.58
Mo–BNNc	5.90	–447.46	–447.46	–447.49	96.55
Pd–BNNc	2.34	–484.50	–484.50	–484.53	102.59
Cd–BNNc	3.98	–435.06	–435.06	–435.09	106.19
$H_2 \rightarrow$ Cr–BNNc	4.98	–459.92	–459.92	–459.95	99.46
$H_2 \rightarrow$ Ni–BNNc	2.71	–511.96	–511.96	–511.99	103.47
$H_2 \rightarrow$ Zn–BNNc	4.67	–446.84	–446.84	–446.87	104.10
$H_2 \rightarrow$ Mo–BNNc	7.75	–448.18	–448.18	–448.21	96.77
$H_2 \rightarrow$ Pd–BNNc	3.17	–485.22	–485.22	–485.25	102.08
$H_2 \rightarrow$ Cd–BNNc	5.14	–435.78	–435.78	–435.81	105.28

tron potency of doped Cr, Ni, Zn, Mo, Pd, Cd on the BNNc. The doped nanocage of Zn–BNNc (Fig. 5c) and Cd–BNNc (Fig. 5f) has shown the lowest fluctuations and the lowest tendency for adsorption of H_2 molecules than Cr–BNNc, Ni–BNNc, Mo–BNNc, and Pd–BNNc complexes, respectively, (Figs. 5a, 5b, 5d, 5e). Therefore, it can be found that IR spectroscopy of H_2-adsorbed Ni–BNNc (Fig. 5b) and Pd–BNNc (Fig. 5e) with two notable sharp peaks are now well-placed to address specific questions on the individual effect of charge carriers (hydrogen molecule-nanocage), as well as doping atoms on the overall structure. Table 3 through the thermodynamic specifications concluded that (Cr, Ni, Zn, Mo, Pd, Cd)–BNNc due to adsorption of H_2 might be more efficient molecules for absorbing the hydrogen.

Thermodynamic parameters of H_2 molecules adsorption on the (Cr, Ni, Zn, Mo, Pd, Cd)–BNNc complexes have been determined using DFT theoretical technique. It has been shown that for a given number of hydrogen donor sites in H_2 molecules, the stabilities of complexes owing to doping atoms of Cr, Ni, Zn, Mo, Pd, Cd can be considered as:

$$\text{Ni–BNNc} > \text{Pd–BNNc} \gg \text{Cr–BNNc} > \text{Mo–BNNc} \approx \text{Zn–BNNc} > \text{Cd–BNNc},$$

complexes (Table 3). It has been detected the maximum efficiency of Cr, Ni, Zn, Mo, Pd, Cd atoms doping of BNNc pristine for H_2 molecules adsorption through ΔG^{o}_{ads} which depends on the covalent bond between H_2 molecules and (Cr, Ni, Zn, Mo, Pd, Cd)–BNNc.

The adsorption process of H_2 molecules on the (Cr, Ni, Zn, Mo, Pd, Cd)–BNNc is affirmed by the ΔG^{o}_{ads} quantities:

$$\Delta G^{o}_{ads} = \Delta G^{o}_{H2\rightarrow(Cr,\ Ni,\ Zn,\ Mo,\ Pd,\ Cd)-BNNc} - \left(\Delta G^{o}_{H2} + \Delta G^{o}_{(Cr,\ Ni,\ Zn,\ Mo,\ Pd,\ Cd)-BNNc} + \Delta G^{o}_{BNNc}\right).$$

Table 3 has shown the key role of doped Cr, Ni, Zn, Mo, Pd, Cd during interaction between the adsorbate of H_2 molecules as the electron donors and the adsorbent of Cr–BNNc, Ni–BNNc, Zn–BNNc, Mo–BNNc, Pd–BNNc, and Cd–BNNc nanocages as electron acceptors. Therefore, the selectivity of atom-doped on boron nitride nanocage for H_2 adsorption can be resulted as:

$$\text{Ni} > \text{Pd} \gg \text{Cr} > \text{Mo} \approx \text{Zn} > \text{Cd},$$

complexes (Table 3).

Stability Energy and Electron Localization Function Analysis

Then, the adsorption of hydrogen molecules on the BNNc was studied while all boron atoms were substituted with transition metals of Cr, Ni, Zn, Mo, Pd, Cd towards formation of Cr_5N_{10}, Ni_5N_{10}, Zn_5N_{10}, Mo_5N_{10}, Pd_5N_{10}, Cd_5N_{10} nanocages. Therefore, the appreciable adsorption energy and dipole moment, influenced by the different geometrical orientation of the hydrogen molecule relative to the reaction site on the TM (Cr, Ni, Zn, Mo, Pd, Cd) doping site based on the bond angle of N11–TM13–H16 has been investi-

Table 4. Stability energy and dipole moment of hydrogen adsorption on the surface of Cr_5N_{10}, Ni_5N_{10}, Zn_5N_{10}, Mo_5N_{10}, Pd_5N_{10}, Cd_5N_{10} nanocages in different geometrical orientation based on bond angle of N11–TM13–H16

Nanocages	$E \times 10^{-3}$, kcal mol^{-1}	D, debye	$E \times 10^{-3}$, kcal mol^{-1}	D, debye	$E \times 10^{-3}$, kcal mol^{-1}	D, debye
N11–TM13–H16	90°		120°		180°	
$H_2 \rightarrow Cr_5N_{10}$	−614.08	1.87	−614.07	2.29	−614.07	2.76
$H_2 \rightarrow Ni_5N_{10}$	−874.22	1.58	−874.23	1.79	−874.22	1.22
$H_2 \rightarrow Zn_5N_{10}$	−548.49	2.62	−548.51	2.53	−548.50	2.49
$H_2 \rightarrow Mo_5N_{10}$	−555.38	3.08	−555.37	3.55	−555.37	3.80
$H_2 \rightarrow Pd_5N_{10}$	−740.55	2.35	−740.55	1.99	−740.56	1.62
$H_2 \rightarrow Cd_5N_{10}$	−493.25	2.55	−493.25	2.37	−493.26	2.25

TM = (Cr, Ni, Zn, Mo, Pd, Cd).

gated (Table 4). It has been indicated that the stabilities of hydrated nanocages can be evaluated as:

$$H_2 \rightarrow Ni_5N_{10} > H_2 \rightarrow Pd_5N_{10} \gg H_2 \rightarrow Cr_5N_{10} > H_2 \rightarrow Mo_5N_{10} \approx H_2 \rightarrow Zn_5N_{10} > H_2 \rightarrow Cd_5N_{10},$$

considering different adsorption orientation (Table 4).

A type of scalar fields called electron localization function (ELF) may demonstrate a broad span of bonding samples. Nevertheless, the distinction between deduced/raised electron delocalization/localization into cyclic π-conjugated sets stays encouraging for ELF [72]. The grosser the electron localization is in an area, the more likely the electron movement is restricted within it. Therefore, they might be discerned from the ones away if electrons are totally centralized. As Bader investigated, the zones with large electron localization possess extensive magnitudes of Fermi hole integration. But, with having a six-dimension function for the Fermi hole, it seems hard to be studied directly. Then, Becke and Edgecombe remarked that spherically averaged like spin conditional pair probability possesses a direct correlation with the Fermi hole and proposed the parameter of ELF in Multiwfn program [48] and popularized for spin-polarized procedure [73]. Regarding kinetic energy, ELF was rechecked to be more punctual for both Kohn-Sham DFT and post-HF wavefunctions [74].

Adsorption of hydrogen molecules by different geometrical orientation (90°, 120°, 180°) on the nanocages of Cr_5N_{10}, Ni_5N_{10}, Zn_5N_{10}, Mo_5N_{10}, Pd_5N_{10}, Cd_5N_{10} can be defined by ELF graphs owing to exploring their delocalization/localization characterizations of electrons and chemical bonds (Fig. 6). A vaster jointed area engaged by an isosurface map for $H_2 \rightarrow Cr_5N_{10}$ with optimized adsorption at 90° (Fig. 6a), $H_2 \rightarrow Ni_5N_{10}$ with optimized adsorption at 120°(Fig. 6b), $H_2 \rightarrow Zn_5N_{10}$ with optimized adsorption at 120° (Fig. 6c), $H_2 \rightarrow Mo_5N_{10}$ with optimized adsorption at 90° (Fig. 6d), $H_2 \rightarrow Pd_5N_{10}$ with optimized adsorption at 180° (Fig. 6e), and $H_2 \rightarrow Cd_5N_{10}$ with optimized adsorption at 180° (Fig. 6f) means that electron delocalization in these nanoclusters is easier than other geometrical orientations through labeling atoms of N11, Cr13, Ni13, Zn13, Mo13, Pd13, Cd13 and H16.

CONCLUSIONS

This research has investigated doping of (Cr, Ni, Zn, Mo, Pd, Cd) elements on the boron nitride nanocage (BNNc) for enhancing H_2 sensing applying in the hydrogen-based energy storage technology. Therefore, H_2 molecules adsorption involving the (Cr, Ni, Zn, Mo, Pd, Cd)–BNNc nanocages has been experimented based on electrostatic interactions between the H_2 molecules and (Cr, Ni, Zn, Mo, Pd, Cd)–BNNc complexes. The PDOS can evaluate a determined charge assembly between hydrogen molecules and (Cr, Ni, Zn, Mo, Pd, Cd)–BNNc which indicates the competition among transitions metals consisting of chromium, nickel, zinc, molybdenum, palladium, and cadmium. Based on NQR analysis, nickel and palladium with atomic charges of 0.2658 and 0.3266 coulomb on the complexes of Ni–BNNc and Pd–BNNc, respectively, have shown much more tendency for H_2 adsorption than other complexes. The electromagnetic and thermodynamic properties of (Cr, Ni, Zn, Mo, Pd, Cd)–BNNc complexes were computed using density functional theory. The results have illustrated that chosen hydrogen molecules adsorbed on the (Cr, Ni, Zn, Mo, Pd, Cd)–BNNc are rather stable with the most stable adsorption site being in the center of (Cr, Ni, Zn, Mo, Pd, Cd)–BNNc system. The selectivity of atom-doped on boron nitride nanocage for H_2 molecules adsorption can be resulted as:

$$Ni–BNNc > Pd–BNNc \gg Cr–BNNc > Mo–BNNc \approx Zn–BNNc > Cd–BNNc,$$

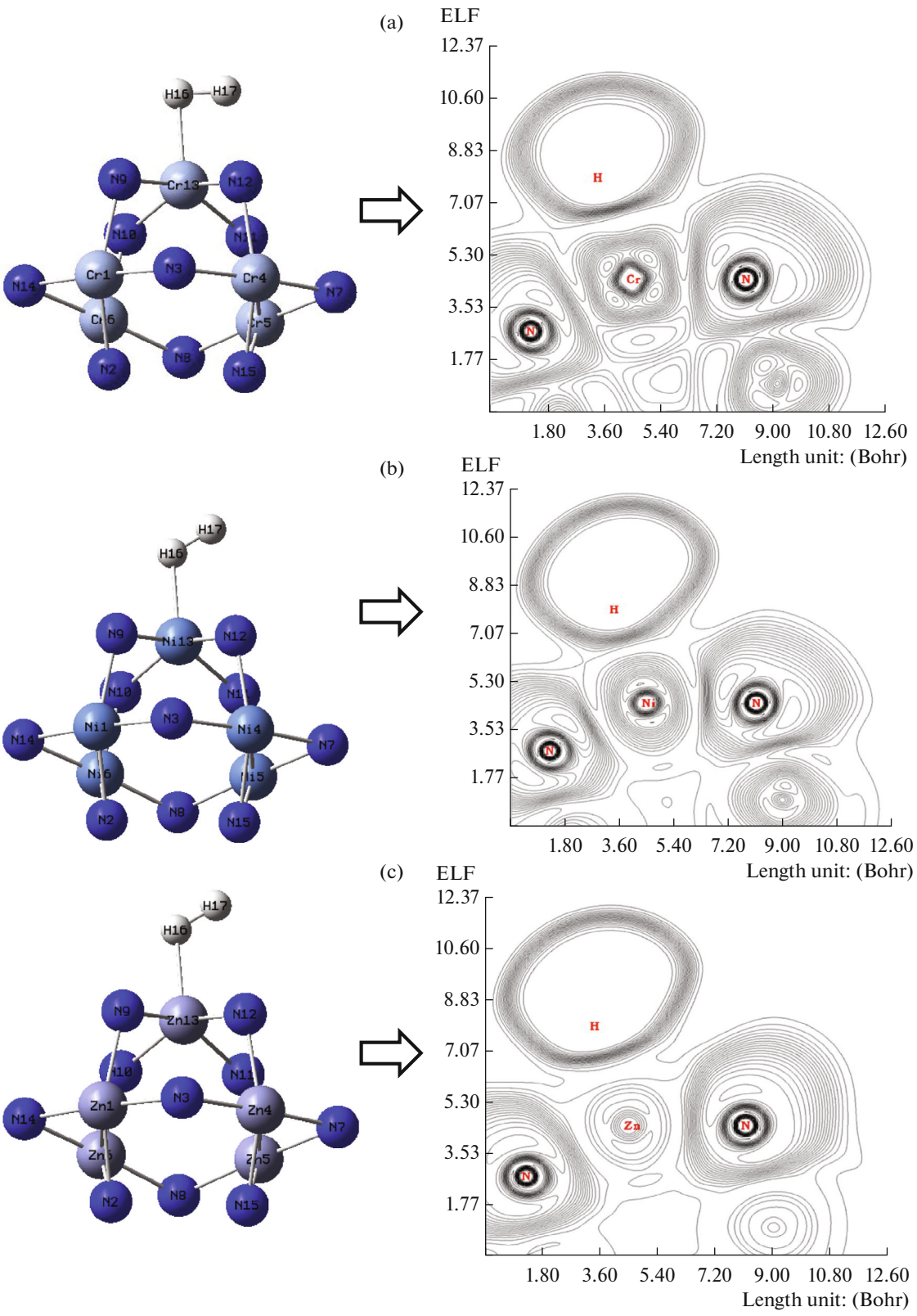

Fig. 6. The Counter line map of electron localization function (ELF) for (a) $H_2 \rightarrow Cr_5N_{10}$, (b) $H_2 \rightarrow Ni_5N_{10}$, (c) $H_2 \rightarrow Zn_5N_{10}$, (d) $H_2 \rightarrow Mo_5N_{10}$, (e) $H_2 \rightarrow Pd_5N_{10}$, and (f) $H_2 \rightarrow Cd_5N_{10}$ nanocages.

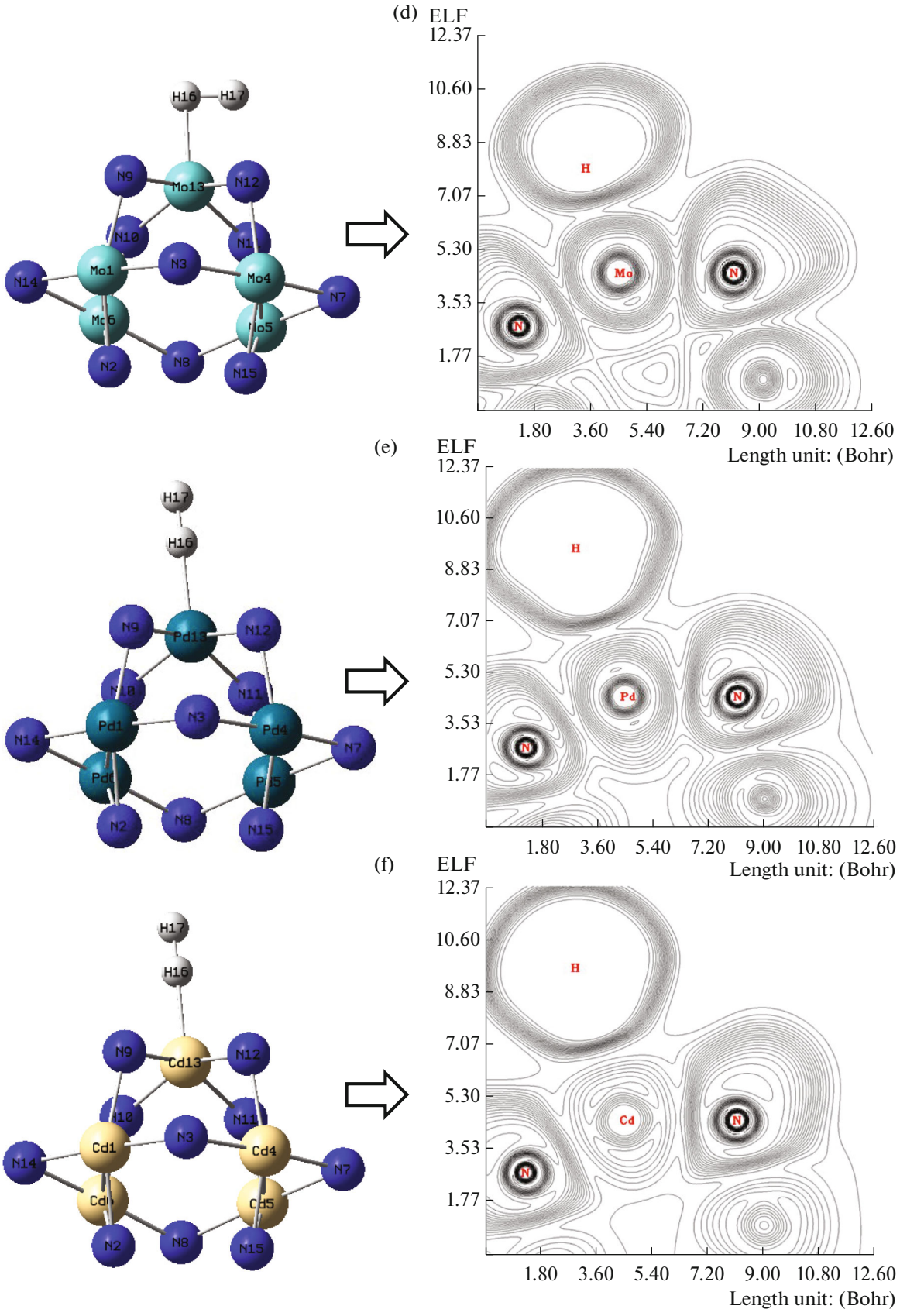
(d)
ELF
12.37
10.60
8.83
7.07
5.30
3.53
1.77
H16
H17
N9
Mo13
N12
N10
N11
Mo1
N3
Mo4
N14
N7
Mo6
Mo5
N2
N8
N15
H
Mo
N
1.80 3.60 5.40 7.20 9.00 10.80 12.60
Length unit: (Bohr)
(e)
ELF
12.37
10.60
8.83
7.07
5.30
3.53
1.77
H17
H16
N9
Pd13
N12
N11
Pd1
N3
Pd4
N14
N7
N2
N8
N15
H
Pd
N
1.80 3.60 5.40 7.20 9.00 10.80 12.60
Length unit: (Bohr)
(f)
ELF
12.37
10.60
8.83
7.07
5.30
3.53
1.77
H17
H16
N9
Cd13
N12
N11
N3
Cd1
Cd4
N14
N7
Cd5
N2
N8
N15
H
Cd
N
1.80 3.60 5.40 7.20 9.00 10.80 12.60
Length unit: (Bohr)

Fig. 6. (Contd.)

complexes, respectively. This work proposes that transition metals as ferromagnetic semiconductor can be examined through doping on the nanomaterials for enhancing the adsorption potency.

ACKNOWLEDGMENTS

In successfully completing this paper and its research, the authors are grateful to Kastamonu University.

FUNDING

This work was supported by ongoing institutional funding. No additional grants to carry out or direct this particular research were obtained.

CONFLICT OF INTEREST

The authors of this work declare that they have no conflicts of interest.

REFERENCES

1. H. Ran, J. Yin, and H. Li, Nanomaterials **13**, 584 (2023). https://doi.org/10.3390/nano13030584
2. F. Mollaamin and M. Monajjemi, Comput. Theor. Chem. **1237**, 114666 (2024). https://doi.org/10.1016/j.comptc.2024.114666
3. E. A. Lebedeva, S. A. Astaf'eva, and T. S. Istomina, Russ. J. Phys. Chem. B **16**, 316–322 (2022). https://doi.org/10.1134/S1990793122010109
4. F. Mollaamin and M.Monajjemi, J. Mol. Struct. **1300**, 137214 (2024). https://doi.org/10.1016/j.molstruc.2023.137214
5. D. V. Shtansky, A. T. Matveev, E. S. Permyakova, et al., Nanomaterials **12**, 2810 (2022). https://doi.org/10.3390/nano12162810
6. Y. Yang, Y. Peng, M. F. Saleem, et al., Materials **15**, 4396 (2022). https://doi.org/10.3390/ma15134396
7. A. Davies, J. D. Albar, A. Summerfield, et al., Nano Lett. **18**, 498–504 (2018). https://doi.org/10.1021/acs.nanolett.7b04453
8. F. Mollaamin and M. Monajjemi, Sens. Rev. **44**, 179–193 (2024). https://doi.org/10.1108/SR-01-2024-0066
9. Y. H. Chao, J. Zhang, H. P. Li, et al., Chem. Eng. J. **387**, 124138 (2020). https://doi.org/10.1016/j.cej.2020.124138
10. F. Mollaamin, S. Mohammadi, Z. Khalaj, et al., Russ. J. Phys. Chem. B **18**, 67–82 (2024). https://doi.org/10.1134/S1990793124010330
11. N. V. Dokhlikova, S. A. Ozerin, S. V. Doronin, et al., Russ. J. Phys. Chem. B **16**, 461–467 (2022). https://doi.org/10.1134/S1990793122030137
12. Y. Guo, R. X. Wang, P. F. Wang, et al., ACS Sustainable Chem. Eng. **7**, 5727–5741 (2019). https://doi.org/10.1021/ACSSUSCHEMENG.8B05150
13. M. I. Ikim, E. Y. Spiridonova, V. F. Gromov, et al., Russ. J. Phys. Chem. B **17**, 774–777 (2023). https://doi.org/10.1134/S199079312303003X
14. N. V. Dokhlikova, A. K. Gatin, S. Y. Sarvadiy, et al., J. Phys. Chem. B **16**, 361–369 (2022). https://doi.org/10.1134/S1990793122020166
15. K. Y. Troshin, N. M. Rubtsov, G. I. Tsvetkov, et al., Russ. J. Phys. Chem. B **17**, 979–985 (2023). https://doi.org/10.1134/S1990793123040310
16. F. Mollaamin and M. Monajjemi, Russ. J. Phys. Chem. B **18**, 49–66 (2024). https://doi.org/10.1134/S1990793124010159
17. E. I. Rudenko, N. V. Dohlikova, A. K. Gatin, et al., Russ. J. Phys. Chem. B **17**, 845–852 (2023). https://doi.org/10.1134/S1990793123040164
18. A. M. Tereza, G. L. Agafonov, E. K. Anderzhanov, et al., Russ. J. Phys. Chem. B **17**, 974–978 (2023). https://doi.org/10.1134/S1990793123040309
19. M. A. Kotov, S. Y. Lavrentyev, N. G. Solovyov, et al., Russ. J. Phys. Chem. B **17**, 953–961 (2023). https://doi.org/10.1134/S1990793123040267
20. F. Mollaamin and M. Monajjemi, Russ. J. Phys. Chem. B **18**, 607–623 (2024). https://doi.org/10.1134/S1990793124020271
21. M. Monajjemi, F. Mollaamin, and S. Shojaei, Biointerface Res. Appl. Chem. **10**, 5575 (2020). https://doi.org/10.33263/BRIAC103.575585
22. S. Shahriari, F. Mollaamin, and M. Monajjemi, Micromachines **14**, 241 (2023). https://doi.org/10.3390/mi14020241
23. F. Mollaamin and M. Monajjemi, Russ. J. Phys. Chem. B **17**, 658–672 (2023). https://doi.org/10.1134/S1990793123030223
24. F. Mollaamin and M. Monajjemi, Russ. J. Phys. Chem. B **18**, 398–418 (2024). https://doi.org/10.1134/S199079312402026X
25. B. Khalili Hadad, F. Mollaamin, and M. Monajjemi, Russ. Chem. Bull. **60**, 238–241 (2011). https://doi.org/10.1007/s11172-011-0039-5
26. M. Monajjemi, L. Mahdavian, F. Mollaamin, et al., Russ. J. Inorg. Chem. **54**, 1465–1473 (2009). https://doi.org/10.1134/S0036023609090216
27. A. Tahan, F. Mollaamin, and M. Monajjemi, Russ. J. Phys. Chem. **83**, 587–597 (2009). https://doi.org/10.1134/S003602440904013X
28. F. Mollaamin and M. Monajjemi, Russ. J. Phys. Chem. B **18**, 805–820 (2024). https://doi.org/10.1134/S1990793124700131
29. M. Monajjemi, M. T. Baie, and F. Mollaamin, Russ. Chem. Bull. **59**, 886–889 (2010). https://doi.org/10.1007/s11172-010-0181-5
30. S. Shahriari, M. Monajjemi, and F. Mollaamin, J. Chil. Chem. Soc. **67**, 5468–5476 (2022). https://doi.org/10.4067/S0717-97072022000205468
31. M. A. A. Zadeh, H. Lari, L. Kharghanian, et al., J. Comput. Theor. Nanosci. **12**, 4358 (2015). https://doi.org/10.1166/jctn.2015.4366
32. S. Chahal, T. Kumar Sahu, S. Kar, et al., J. Phys. Chem. C **126**, 21084–21093 (2022). https://doi.org/10.1021/acs.jpcc.2c06693

33. E. M. Sarasia, S. Afsharnezhad, B. Honarparvar, et al., Phys. Chem. Liq. **49**, 561–571 (2011). https://doi.org/10.1080/00319101003698992
34. S. Shahriari, M. Monajjemi, and K. Zare, Biointerface Res. Appl. Chem. **8**, 3219–3223 (2018)
35. M. Khaleghian, M. Zahmatkesh, F. Mollaamin, et al., Fullerenes, Nanotubes Carbon Nanostruct. **19**, 251–261 (2011). https://doi.org/10.1080/15363831003721757
36. F Mollaamin and M. Monajjemi, J. Comput. Theor. Nanosci. **12**, 1030–1039 (2015). https://doi.org/10.1166/jctn.2015.3846
37. K. Bakhshi, F. Mollaamin, and M. Monajjemi, J. Comput. Theor. Nanosci. **8**, 763–768 (2011). https://doi.org/10.1166/jctn.2011.1750
38. F. Mollaamin, M. Monajjemi, S. Salemi, et al., Fullerenes, Nanotubes Carbon Nanostruct. **19**, 182 (2011). https://doi.org/10.1080/15363831003782932
39. M. Monajjemi, M. Khaleghian, N. Tadayonpour, et al., Int. J. Nanosci. **09**, 517–529 (2010). https://doi.org/10.1142/S0219581X10007071
40. F. Mollaamin and M. Monajjemi, J. Cluster Sci. **34**, 2901 (2023). https://doi.org/10.1007/s10876-023-02436-5
41. F. Mollaamin and M. Monajjemi, J. Mol. Model. **29**, 119 (2023). https://doi.org/10.1007/s00894-023-05526-3
42. J. P. Perdew, K. Burke, and M. Ernzerhof, Phys. Rev. Lett. **77**, 3865 (1996). https://doi.org/10.1103/PhysRevLett.77.3865
43. R. Alaya, K. Kourchid, Y. Althaqafi, et al., Russ. J. Phys. Chem. B **17**, 868–877 (2023). https://doi.org/10.1134/S1990793123040024
44. X. Yuan, X. Tan, and B. Liu, Russ. J. Phys. Chem. B **17**, 886–895 (2023). https://doi.org/10.1134/S1990793123040322
45. P. Hohenberg and W. Kohn, Phys. Rev. B **136**, B864–B871 (1964). https://doi.org/10.1103/PhysRev.136.B864
46. W. Kohn and L. J. Sham, Phys. Rev. **140**, A1133–A1138 (1965). https://doi.org/10.1103/PhysRev.140.A1133
47. A. D. Becke, J. Chem. Phys. **98**, 5648–5652 (1993). https://doi.org/10.1063/1.464913
48. C. Lee, W. Yang, and R. G. Parr, Phys. Rev. B **37**, 785–789 (1988). https://doi.org/10.1103/PhysRevB.37.785
49. K. Kim and K. D. Jordan, J. Phys. Chem. **98**, 10089–10094 (1994). https://doi.org/10.1021/j100091a024
50. P. J. Stephens, F. J. Devlin, C. F. Chabalowski, et al., J. Phys. Chem. **98**, 11623–11627 (1994). https://doi.org/10.1021/j100096a001
51. C. J. Cramer, *Essentials of Computational Chemistry: Theories and Models*, 2nd ed. (Wiley, Hoboken, NJ, 2004). https://www.wiley.com. Accessed June 24, 2021.
52. F. Mollaamin and M. Monajjemi, Int. J. Quantum Chem. **124**, e27348 (2024). https://doi.org/10.1002/qua.27348
53. F. Mollaamin and M. Monajjemi, Mol. Simul. **49**, 365 (2023). https://doi.org/10.1080/08927022.2022.2159996
54. S. H. Touhami, K. Almi, S. Lakel, et al., Russ. J. Phys. Chem. B **17**, 1057–1068 (2023). https://doi.org/10.1134/S1990793123050287
55. M. J. Frisch, G. W. Trucks, H. B. Schlegel, G. E. Scuseria, M. A. Robb, J. R. Cheeseman, G. Scalmani, V. Barone, G. A. Petersson, H. Nakatsuji, X. Li, M. Caricato, A. V. Marenich, J. Bloino, B. G. Janesko, R. Gomperts, B. Mennucci, H. P. Hratchian, J. V. Ortiz, A. F. Izmaylov, J. L. Sonnenberg, D. Williams-Young, F. Ding, F. Lipparini, F. Egidi, J. Goings, B. Peng, A. Petrone, T. Henderson, D. Ranasinghe, V. G. Zakrzewski, J. Gao, N. Rega, G. Zheng, W. Liang, M. Hada, M. Ehara, K. Toyota, R. Fukuda, J. Hasegawa, M. Ishida, T. Nakajima, Y. Honda, O. Kitao, H. Nakai, T. Vreven, K. Throssell, J. A. Montgomery, Jr., J. E. Peralta, F. Ogliaro, M. J. Bearpark, J. J. Heyd, E. N. Brothers, K. N. Kudin, V. N. Staroverov, T. A. Keith, R. Kobayashi, J. Normand, K. Raghavachari, A. P. Rendell, J. C. Burant, S. S. Iyengar, J. Tomasi, M. Cossi, J. M. Millam, M. Klene, C. Adamo, R. Cammi, J. W. Ochterski, R. L. Martin, K. Morokuma, O. Farkas, J. B. Foresman, and D. J. Fox, Gaussian 16, Revision C.01, Gaussian, Inc., Wallingford CT, 2016.
56. R. Dennington, T. A. Keith, and J. M. Millam, *GaussView, Version 6.06.16* (Semichem Inc., Shawnee Mission, KS, 2016).
57. F. Mollaamin, J. Comput. Theor. Nanosci. **11**, 2393–2398 (2014). https://doi.org/10.1166/jctn.2014.3653
58. F. Mollaamin, A. Ilkhani, N. Sakhaei, et al., J. Comput. Theor. Nanosci. **12**, 3148–3154 (2015). https://doi.org/10.1166/jctn.2015.4092
59. F. Mollaamin and M. Monajjemi, J. Mol. Model. **29**, 170 (2023). https://doi.org/10.1007/s00894-023-05567-8
60. F. Mollaamin, S. Shahriari, M. Monajjemi, et al., J. Cluster Sci. **34**, 1547–1562 (2023). https://doi.org/10.1007/s10876-022-02335-1
61. Z. Trontelj, J. Pirnat, V. Jazbinšek, et al., Crystals **10**, 450 (2020). https://doi.org/10.3390/cryst10060450
62. R. Sciotto, I. A. Ruiz Alvarado, and W. G. Schmidt, Surfaces **7**, 79–87 (2024). https://doi.org/10.3390/surfaces7010006
63. J. Luo, C. Wang, Z. Wang, et al., Chin. Phys. B **29**, 067402 (2020). https://doi.org/10.1088/1674-1056/ab892d
64. H. A. Young and R. D. Freedman, *Sears and Zemansky's University Physics with Modern Physics*, 13th ed. (Addison-Wesley, Boston, 2012), p. 754.
65. A. G. Chetverikova, V. L. Berdinsky, O. N. Kanygina, et al., Russ. J. Phys. Chem. B **18**, 378–387 (2024). https://doi.org/10.1134/S1990793124020052
66. P. A. Purtov, Russ. J. Phys. Chem. B **18**, 23–27 (2024). https://doi.org/10.1134/S1990793124010366
67. I. Asfour, Russ. J. Phys. Chem. B **18**, 83–94 (2024). https://doi.org/10.1134/S1990793124010032

68. A. L. Buchachenko, Russ. J. Phys. Chem. B **18**, 229–238 (2024). https://doi.org/10.1134/S1990793124010068
69. V. E. Kirillov, G. Y. Yurkov, M. S. Korobov, et al., Russ. J. Phys. Chem. B **17**, 1346–1354 (2023). https://doi.org/10.1134/S1990793123060040
70. E. V. Morozov, A. V. Il'ichev, and V. M. Bouznik, Russ. J. Phys. Chem. B **17**, 1361–1369 (2023). https://doi.org/10.1134/S1990793123060064
71. A. A. Shmyreva, V. E. Kirillov, E. B. Dzhangurazov, et al., Russ. J. Phys. Chem. B **17**, 764–773 (2023). https://doi.org/10.1134/S1990793123030120
72. C. F. Matta, P. W. Ayers, and R. Cook, "The physics of electron localization and delocalization," in *Electron Localization-Delocalization Matrices. Lecture Notes in Chemistry* (Springer, Cham, 2024), Vol. 112. https://doi.org/10.1007/978-3-031-51434-0_2
73. Z. Trontelj, J. Pirnat, V. Jazbinšek, et al., Crystals **10**, 450 (2020). https://doi.org/10.3390/cryst10060450
74. R. Sciotto, I. A. Ruiz Alvarado, and W. G. Schmidt, Surfaces **7**, 79–87 (2024). https://doi.org/10.3390/surfaces7010006